Mixed Ruthenium−Rhodium Carbonyl Clusters. Synthesis and Crystal Structure of the $[PPh_4]^+$ Salts of the Anions $[Ru_2Rh_2(CO)_7(\mu\text{-}CO)_5]^{2-}$, $[Ru_2Rh_2(CO)_9(\mu\text{-}CO)_3(\mu\text{-}H)]^-$, and $[Ru_2Rh_2(CO)_7(\mu\text{-}CO)_5(\mu_3\text{-}AuPPh_3)]^-$ †

Alessandro Fumagalli,*[1a] Davide Italia,[1b] Maria Carlotta Malatesta,[1b] Gianfranco Ciani,[1c] Massimo Moret,[1c] and Angelo Sironi*[1c]

CNR-Centro di Studio sulla Sintesi e la Struttura dei Composti dei Metalli di Transizione nei Bassi Stati di Ossidazione, Dipartimento di Chimica Inorganica Metallorganica e Analitica, and Dipartimento di Chimica Strutturale e Stereochimica Inorganica, Università di Milano, Via G. Venezian 21, 20133 Milano, Italy

Received June 8, 1995[⊗]

The anion $[Ru_2Rh_2(CO)_{12}]^{2-}$ (**1**) has been obtained by reaction of $Ru_3(CO)_{12}$ with $[Rh(CO)_4]^-$ as $[N(PPh_3)_2]^+$ or $(PPh_4)^+$ salts; this species reacts with acids or $AuPPh_3Cl$ to give respectively $[Ru_2Rh_2(CO)_{12}H]^-$ (**2**) and $[Ru_2Rh_2(CO)_{12}(AuPPh_3)]^-$ (**3**). The phosphonium salts $(PPh_4)_2[Ru_2Rh_2(CO)_{12}]\cdot THF$ (**I**), $(PPh_4)[Ru_2Rh_2(CO)_{12}H]$ (**II**), and $(PPh_4)[Ru_2Rh_2(CO)_{12}(AuPPh_3)]$ (**III**) were characterized by single-crystal X-ray diffraction: **I**, space group $P2_1/n$, $Z = 4$, $a = 11.256(2)$ Å, $b = 26.712(2)$ Å, $c = 20.048(5)$ Å, $\beta = 90.45(2)°$, R1 = 0.048 for 4049 independent reflections with $I > 3\sigma(I)$; **II** space group $P2_1/a$, $Z = 4$, $a = 12.453(2)$ Å, $b = 24.074(3)$ Å, $c = 13.174(2)$ Å, $\beta = 90.67(1)°$, R1 = 0.039 for 4034 independent reflections with $I > 3\sigma(I)$; **III**, space group $P2_1/n$, $Z = 4$, $a = 11.720(2)$ Å, $b = 13.133(3)$ Å, $c = 35.614(2)$ Å, $\beta = 95.70(1)°$, R1 = 0.054 for 4231 independent reflections with $I > 3\sigma(I)$. Anions **1** and **2** have a tetrahedral Ru_2Rh_2 metal frame, while in **3** there is a trigonal-bipyramidal frame with one ruthenium atom and the gold atom in apical positions; in **2** the H atom bridges the Ru−Ru edge. ^1H and ^{31}P NMR spectra of, respectively, **2** and **3** are consistent with the crystal structures. ^{13}C NMR spectra of both **1** and **2** show evidence of fluxional behavior at 295 K which cannot be frozen at 178 K, where the signals collapse; compound **3** at room temperature shows a partially fluxional solution structure which becomes static at *ca*. 250 K.

Introduction

Several Ru−Rh carbonyl cluster compounds are reported in the literature, many of them containing also hydride, cyclopentadienyl, or phosphine ligands;[2] however, so far, only two homoleptic anionic species have been characterized, $[RuRh_4(CO)_{15}]^{2-}$ [3] and $[RuRh_5(CO)_{16}]^-$.[4] We are particularly interested in the study of equilibria involving metal redistribution between homonuclear and heteronuclear carbonyl cluster species, and a preliminary investigation revealed that the system of Ru, Rh, and Ru−Rh clusters is rather complex, due to the occurrence of several equilibria, mostly between anionic species. The stability of each species and its role in the equilibria depends upon several factors, such as the oxidation state and the presence or absence of a CO atmosphere. The first results of this investigation are here reported.

Results and Discussion

1. Synthesis and Reactivity of the Anion $[Ru_2Rh_2(CO)_{12}]^{2-}$. The reactions of $Ru_3(CO)_{12}$ with the $(PPh_4)^+$ or $[N(PPh_3)_2]^+$ (hereafter PPN^+) salt of $[Rh(CO)_4]^-$, performed with various molar ratios and under different conditions, were closely monitored by IR spectroscopy with use of spectra subtraction techniques to resolve the mixtures of several species which are often obtained. Thus, it was observed that, in all the cases, the first reaction stages are characterized by formation of the new species $[Ru_2Rh_2(CO)_{12}]^{2-}$ (**1**). The formation of **1** occurs at room temperature within minutes, both under nitrogen and CO; there is no IR evidence of precursors, the reaction is independent of the initial relative amounts of the two reactants which, at this early stages of the reaction, are mostly unreacted. The further evolution of the reaction is, however, dependent upon the particular molar ratio $Ru_3(CO)_{12}$:$[Rh(CO)_4]^-$ which, in a whole series of reactions, was varied within the range 1:3 to 1:1; after equilibration times, which at room temperature are a few hours, different results are thus obtained. Particularly, given the proper 1:3 molar ratio, compound **1** may be obtained pure under a nitrogen atmosphere according to the overall stoichiometry (1). This same reaction, if performed under 1 atm of

$$2Ru_3(CO)_{12} + 6[Rh(CO)_4]^- \rightarrow 3[Ru_2Rh_2(CO)_{12}]^{2-} + 12CO \quad (1)$$

CO, yields a mixture of compounds among which $[RuRh_4(CO)_{15}]^{2-}$ [3] could be detected.

At the other extreme of the range, that is for a 1:1 molar ratio of the two reactants, we had evidence of formation, under nitrogen, of a new compound which is derived by further reaction of the first formed $[Ru_2Rh_2(CO)_{12}]^{2-}$ with $Ru_3(CO)_{12}$; its instability has, so far, prevented isolation and further characterization. For any other molar ratio chosen within the (1:1)−(1:3) range, mixtures mostly of unknown compounds are obtained, both under nitrogen and CO.

† $[PPh_4]_2[Ru_2Rh_2(CO)_{12}]$: bis(tetraphenylphosphonium) 1,3;1,4;2,3;2,4;3,4-pentakis(μ-carbonyl)-1,1,2,2,2,3,4-heptacarbonyl-*tetrahedro*-1,2-diruthenium-3,4-dirhodiate. $[PPh_4][Ru_2Rh_2(CO)_{12}H]$: tetraphenylphosphonium 1,2-(μ-hydrido)-1,3;1,4;3,4-tris(μ-carbonyl)-1,1,2,2,2,3,3,4,4-nonacarbonyl-*tetrahedro*-1,2-diruthenium-3,4-dirhodiate. $[PPh_4][Ru_2Rh_2(CO)_{12}(AuPPh_3)]$: tetraphenylphosphonium 1,3,4-(μ_3-triphenylphosphine)aurio)-1,3;1,4;2,3;2,4;3,4-pentakis(μ-carbonyl)-1,1,2,2,2,3,4-heptacarbonyl-*tetrahedro*-1,2-diruthenium-3,4-dirhodiate.

⊗ Abstract published in *Advance ACS Abstracts,* February 15, 1996.

(1) (a) CNR. (b) Dipartimento di Chimica Inorganica, Metallorganica ed Analitica. (c) Dipartimento di Chimica Strutturale e Stereochimica Inorganica.
(2) Kakkonen, H. J.; Ahlgrèn, M.; Pakkanen, T. A.; Pursianen, J. *J. Organomet. Chem*. **1994**, *482*, 279 and references therein.
(3) Fumagalli, A.; Ciani, G. *J. Organomet. Chem*. **1984**, *272*, 91.
(4) Pursianen, J.; Pakkanen, T. A.; Smolander, K. *J. Chem. Soc., Dalton Trans*. **1987**, 781.

0020-1669/96/1335-1765$12.00/0

It must also be noted that, due to the large difference in the oxidation states of $Ru_3(CO)_{12}$ and $[Rh(CO)_4]^-$, their reaction was expected to be a simple redox condensation,[5] yielding at once a species such as $[Ru_3Rh(CO)_x]^-$. The experimental evidence of **1** as the first stable product formed, in any case, suggests reconsideration of eq 1 as the final result of a complex sequence of fragmentations and aggregations with intermediates which are so short-lived that IR spectra show no evidence of their existence.

Pure $[Ru_2Rh_2(CO)_{12}]^{2-}$ (**1**) reacts with 1 atm of CO at room temperature in THF, giving a minor decomposition which may be reversed by switching to a nitrogen atmosphere. IR subtraction techniques allowed us to estimate that under these conditions *ca*. 10% of the product is decomposed with formation of $[Ru(CO)_4]^-$ and an unknown anion. It is reasonable to suggest a fragmentation as reported in eq 2, with formation of a trinuclear species, possibly $[Ru_2Rh(CO)_{11}]^-$, analogous to the reported $[Fe_2Rh(CO)_{11}]^-$.[6]

$$[Ru_2Rh_2(CO)_{12}]^{2-} + 3CO \rightleftarrows [Ru_2Rh(CO)_{11}]^- + [Rh(CO)_4]^- \quad (2)$$

Analogous equilibria have been already described in Rh cluster chemistry,[5,7] and it has been remarked that the left to right direction is connected to an entropy decrease; thus, low temperature favors these reactions. In fact, we could observe, upon freezing at *ca*. −80 °C, a change of the solution color from orange to yellow, which is reversed at room temperature; the clearer color at low temperature suggests the formation of a species with lower nuclearity. However, the most convincing proof was obtained by ^{13}C NMR, which showed that cleavage occurs at low temperature on $[Ru_2Rh_2(CO)_{12}]^{2-}$ by action of CO, with formation of $[Rh(CO)_4]^-$, whose resonance may be easily detected. Raising the temperature causes recondensation, and the same fluxional spectrum detectable under an N_2 atmosphere is obtained.

A moderate excess of strong acid (CF_3COOH, H_2SO_4) (*ca*. 50% over the stoichiometric) is required to produce in THF complete conversion, according to IR, of species **1** to the new hydrido species $[Ru_2Rh_2(CO)_{12}H]^-$ (**2**), which was recovered and structurally characterized (see below). The reaction is simply a protonation:

$$[Ru_2Rh_2(CO)_{12}]^{2-} + H^+ \rightarrow [Ru_2Rh_2(CO)_{12}H]^- \quad (3)$$

The IR spectrum of **2** (see below) shows a shift of the bands in the CO stretching region of *ca*. 60 cm^{-1} toward higher wavenumbers, with respect to **1**, consistent with the reduced anionic charge on the cluster and consequent weakening of M−CO back-donation. The hydrido anion **2** is stable in THF even in the presence of considerable excess acid, and less basic solvents such as CH_2Cl_2 and *n*-hexane are required to give with CF_3COOH the previously reported dihydrido species $[Ru_2Rh_2(CO)_{12}H_2]$.[8]

Very similar is the reaction of **1** with $AuPPh_3Cl$, which gives the new monoanionic gold derivative **3**, isolated and structurally characterized. In this case also, a slight excess of reagent (10−15%) in THF is required to drive to completion the condensation of the $[AuPPh_3]^+$ moiety, according to eq 4.

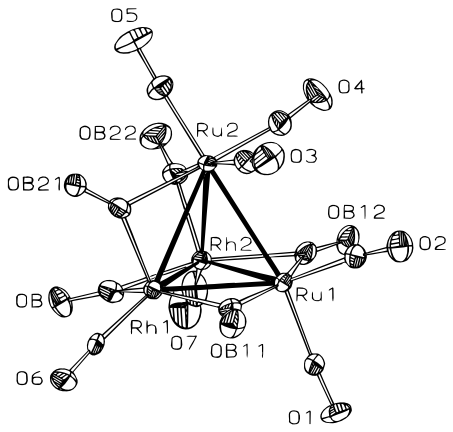

Figure 1. View of the $[Ru_2Rh_2(CO)_7(\mu_2\text{-}CO)_5]^{2-}$ anion (**1**). The C atoms of the carbonyl groups bear the same numbering as the respective O atoms. The anion has C_s idealized symmetry; the mirror plane contains the Ru(1), Ru(2), C(1), O(1), C(2), O(2), C(B), and O(B) atoms.

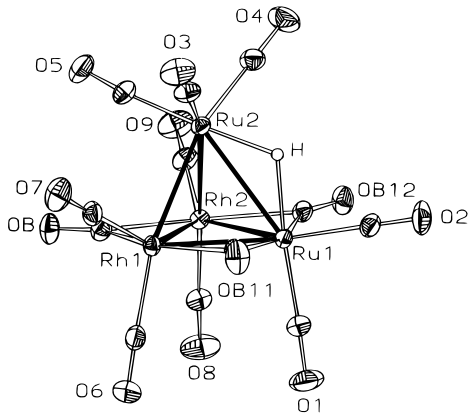

Figure 2. View of the $[Ru_2Rh_2(CO)_9(\mu_2\text{-}CO)_3(\mu_2\text{-}H)]^-$ anion (**2**). The C atoms of the carbonyl groups bear the same numbering as the respective connected O atoms. The anion has C_s idealized symmetry; the mirror plane contains the Ru(1), Ru(2), H, C(1), O(1), C(2), O(2), C(B), and O(B) atoms.

$$[Ru_2Rh_2(CO)_{12}]^{2-} + AuPPh_3Cl \rightarrow [Ru_2Rh_2(CO)_{12}(AuPPh_3)]^- + Cl^- \quad (4)$$

No evidence of a digold neutral derivative was obtained with larger excess of $AuPPh_3Cl$ in THF; this reaction, however, should be more correctly considered as an equilibrium as found in similar cases,[9] and in this respect, the accumulation of Cl^- appears of relevance as a countereffect toward the condensation of a second gold fragment. Comparison of the IR spectrum of **3** with that of species **1** shows a shift of the CO bands toward higher wavenumbers, as found in compound **2**, but in this case the shift is only *ca*. 40 cm^{-1}, due to the minor electrophilicity of $(AuPPh_3)^+$ with respect to H^+.

2. Crystal Structures of $(PPh_4)_2[Ru_2Rh_2(CO)_7(\mu_2\text{-}CO)_5]$, $(PPh_4)[Ru_2Rh_2(CO)_9(\mu_2\text{-}CO)_3(\mu_2\text{-}H)]$, and $(PPh_4)[Ru_2Rh_2(CO)_7(\mu_2\text{-}CO)_5(\mu_3\text{-}AuPPh_3)]$. The three crystal structures consist of a packing of cations and anions, in the proper molar ratio, with normal van der Waals contacts between the atoms of different ionic fragments. Selected bond distances and angles for **I**−**III** are listed in Tables 1−3, respectively. Figures 1−3 report ORTEP plots of anions **1**−**3**, respectively, together with the proper atom-labeling scheme.

(5) Chini, P.; Longoni, G.; Albano, V. G. *Adv. Organomet. Chem.* **1976**, *14*, 285.
(6) Ceriotti, A.; Longoni, G.; Della Pergola, R.; Heaton, B. T.; Smith, D. O. *J. Chem. Soc., Dalton Trans.* **1983**, 1433.
(7) Chini, P. *J. Organomet. Chem.* **1980**, *200*, 39 and references within.
(8) Pursianen, J.; Pakkanen, T. A.; Heaton, B. T.; Seregni, C.; Goodfellow, R. G. *J. Chem. Soc., Dalton Trans.* **1986**, 681.
(9) Fumagalli, A.; Martinengo, S.; Albano, V. G.; Braga, D.; Grepioni, F. *J. Chem. Soc., Dalton Trans.* **1989**, 2343.

Table 1. Selected Bond Lengths (Å) and Angles (deg) for the Anion $[Ru_2Ru_2(CO)_{12}]^{2-}$ (**1**)

Ru(1)−Ru(2)	2.952(2)	Ru(1)−Rh(2)	2.732(2)	Ru(2)−Rh(2)	2.864(2)
Ru(1)−Rh(1)	2.740(2)	Ru(2)−Rh(1)	2.910(2)	Rh(1)−Rh(2)	2.705(2)
Ru(1)−C(1)	1.882(15)	C(1)−O(1)	1.126(13)	Ru(1)−C(1)−O(1)	175.8(13)
Ru(1)−C(2)	1.882(15)	C(2)−O(2)	1.127(14)	Ru(1)−C(2)−O(2)	173.7(13)
Ru(2)−C(3)	1.88(2)	C(3)−O(3)	1.18(2)	Ru(2)−C(3)−O(3)	176.9(14)
Ru(2)−C(4)	1.94(2)	C(4)−O(4)	1.11(2)	Ru(2)−C(4)−O(4)	172.7(16)
Ru(2)−C(5)	1.86(2)	C(5)−O(5)	1.130(14)	Ru(2)−C(5)−O(5)	175.7(15)
Rh(1)−C(6)	1.836(14)	C(6)−O(6)	1.116(13)	Rh(1)−C(6)−O(6)	175.9(11)
Rh(2)−C(7)	1.81(2)	C(7)−O(7)	1.18(2)	Rh(2)−C(7)−O(7)	174.7(15)
Ru(1)−C(B11)	2.05(2)	C(B11)−O(B11)	1.196(14)	Ru(1)−C(B11)−O(B11)	144.7(11)
Ru(1)−C(B11)	2.109(15)			Rh(1)−C(B11)−O(B11)	132.8(11)
Ru(1)−C(B12)	2.085(14)	C(B12)−O(B12)	1.153(13)	Ru(1)−C(B12)−O(B12)	143.7(11)
Rh(2)−C(B12)	2.174(14)			Rh(2)−C(B12)−O(B12)	136.5(11)
Ru(2)−C(B21)	2.261(14)	C(B21)−O(B21)	1.163(14)	Ru(2)−C(B21)−O(B21)	131.4(10)
Rh(1)−C(B21)	1.925(14)			Rh(1)−C(B21)−O(B21)	140.9(11)
Ru(2)−C(B22)	2.34(2)	C(B22)−O(B22)	1.148(15)	Ru(2)−C(B22)−O(B22)	130.5(13)
Rh(2)−C(B22)	1.898(15)			Rh(2)−C(B22)−O(B22)	145.1(15)
Rh(1)−C(B)	2.074(12)	C(B)−O(B)	1.183(13)	Rh(1)−C(B)−O(B)	138.9(11)
Rh(2)−C(B)	2.067(14)			Rh(2)−C(B)−O(B)	139.5(10)
Ru(2)−Ru(1)−C(1)	160.5(4)			Ru(2)−Ru(1)−C(2)	101.1(4)
Ru(1)−Ru(2)−C(3)	76.4(5)			Ru(1)−Ru(2)−C(4)	87.7(5)

Table 2. Selected Bond Lengths (Å) and Angles (deg) for the Anion $[Ru_2Rh_2(CO)_{12}H]^-$ (**2**)

Ru(1)−Ru(2)	2.898(1)	Ru(1)−Rh(2)	2.760(1)	Ru(2)−Rh(2)	2.723(1)
Ru(1)−Rh(1)	2.754(1)	Ru(2)−Rh(1)	2.740(1)	Rh(1)−Rh(2)	2.729(1)
Ru(1)−C(1)	1.853(10)	C(1)−O(1)	1.157(11)	Ru(1)−C(1)−O(1)	178.0(10)
Ru(1)−C(2)	1.890(10)	C(2)−O(2)	1.125(11)	Ru(1)−C(2)−O(2)	179.6(9)
Ru(2)−C(3)	1.919(10)	C(3)−O(3)	1.131(11)	Ru(2)−C(3)−O(3)	178.0(10)
Ru(2)−C(4)	1.882(11)	C(4)−O(4)	1.135(11)	Ru(2)−C(4)−O(4)	177.9(11)
Ru(2)−C(5)	1.885(11)	C(5)−O(5)	1.113(11)	Ru(2)−C(5)−O(5)	174.6(10)
Rh(1)−C(6)	1.923(10)	C(6)−O(6)	1.130(11)	Rh(1)−C(6)−O(6)	178.7(10)
Rh(1)−C(7)	1.931(12)	C(7)−O(7)	1.130(12)	Rh(1)−C(7)−O(7)	175.9(11)
Rh(2)−C(8)	1.885(10)	C(8)−O(8)	1.123(10)	Rh(2)−C(8)−O(8)	178.5(10)
Rh(2)−C(9)	1.910(10)	C(9)−O(9)	1.125(11)	Rh(2)−C(9)−O(9)	178.3(10)
Ru(1)−C(B11)	2.046(10)	C(B11)−O(B11)	1.159(10)	Ru(1)−C(B11)−O(B11)	147.7(8)
Rh(1)−C(B11)	2.208(9)			Rh(1)−C(B11)−O(B11)	131.7(7)
Ru(1)−C(B12)	2.101(9)	C(B12)−O(B12)	1.147(9)	Ru(1)−C(B12)−O(B12)	144.5(8)
Rh(2)−C(B12)	2.128(9)			Rh(2)−C(B12)−O(B12)	134.0(8)
Rh(1)−C(B)	2.084(9)	C(B)−O(B)	1.148(10)	Rh(1)−C(B)−O(B)	142.7(8)
Rh(2)−C(B)	2.168(10)			Rh(2)−C(B)−O(B)	137.4(8)
Ru(2)−Ru(1)−C(1)	150.5(3)			Ru(2)−Ru(1)−C(2)	117.3(3)
Ru(1)−Ru(2)−C(3)	108.4(3)			Ru(1)−Ru(2)−C(4)	106.1(3)

It must be noted that rhodium and ruthenium can hardly be differentiated on the basis of their X-ray scattering powers, since they differ by just 1 electron out ouf 45; on the other hand, neutron and/or near-edge synchrotron radiation diffraction experiments, which could discriminate between atoms with a close *Z* value, are not commonly available. However, a difference of one valence electron on one site may be enough to induce significant perturbations of the overall cluster stereogeometry, which eventually allows discrimination between two metal atoms on stereochemical grounds. The comparison of both the local electron bookkeeping and the local stereogeometry of the pertinent atoms can lead to the correct labeling of metal centers, not distinguishable on the basis of even good-quality X-ary diffraction data alone. The presence of a carbonyl semibridging two different metals with similar local stereogeometry is particularly informative since the electron poorer metal, in order to fulfill its ideal EAN and/or to better spread its formal local charge,[10] is expected to have the shortest inteaction. The Rh/Ru labels for the species **1**−**3** have been unambiguously derived using this methodology which, even if somewhat trivial, is not as widespread as it should be. For instance, the closely related tetrahedral cluster $[Ru_2Rh_2(CO)_9(\mu_2\text{-}CO)_3(\mu_2\text{-}H)_2]$[8] has been proposed to have in the solid state a Ru−Rh disorder on two basal sites with similar local stereogeometry, then labeled M(2) and M(3). However, since the carbonyl bridging the M(2)−M(3) edge is semibridging (M(2)−C(11) = 2.132(5) Å *vs* M(3)−C(11) = 2.216(5) Å), the ordered alternative (M(2) = Ru and M(3) = Rh) seems more reasonable. Similar arguments previously led to the reformulation[11] of the disorder present in $[Fe_4CoRhC(CO)_{16}]$.[12]

$[Ru_2Rh_2(CO)_7(\mu_2\text{-}CO)_5]^{2-}$ shares with $[OsRh_3(CO)_7(\mu_2\text{-}CO)_5]^-$ (**4**)[13] the overall idealized C_s symmetry and the unusual feature of a tetrahedral metal skeleton surrounded by seven terminal carbonyls and five carbonyls bridging all but one of the M−M edges. The ligand configuration of the archetypical $[Rh_4(CO)_{12}]$[14] (of C_{3v} symmetry) may be ideally related to the present one by the bending of two terminal equatorial COs toward the apical metal atom to become semibridging; this causes the tilting of the apical $M(CO)_3$ moiety toward the basal Ru1 atom (Ru(1)−Ru(2)−C(3) = 76.4(5)° and Ru(1)−Ru(2)−C(4) = 87.7(5)°) and the lengthening of the Ru(1)−Ru(2) bond (2.951(1) Å). The structural similarity between **1** and **4** and the high M−C connectivity of this same apical atom confirm its assignment as ruthenium (Ru(2)), while the second ruthenium

(10) Sironi, A. *Inorg. Chem.* **1995**, *34*, 1342.

(11) Sironi, A. *Inorg. Chem.* **1992**, *31*, 2467.

(12) Lopatin, V. E.; Gubin, S. P.; Mikova, N. M.; Tsybenov, M. T.; Slovokhotov, Y. L.; Struchkov, Y. T. *J. Organomet. Chem.* **1985**, *292*, 275.

Table 3. Selected Bond Lengths (Å) and Angles (deg) for the Anion $[Ru_2Rh_2(CO)_{12}(AuPPh_3)]^-$ (**3**)

Ru(1)−Ru(2)	3.028(2)	Ru(1)−Au	2.808(2)	Rh(1)−Rh(2)	2.696(2)
Ru(1)−Rh(1)	2.743(2)	Ru(2)−Rh(1)	2.884(2)	Rh(1)−Au	2.833(2)
Ru(1)−Rh(2)	2.738(2)	Ru(2)−Rh(2)	2.880(2)	Rh(2)−Au	2.828(2)
Ru(1)−C(1)	1.86(2)	C(1)−O(1)	1.15(2)	Ru(1)−C(1)−O(1)	178(2)
Ru(1)−C(2)	1.85(2)	C(2)−O(2)	1.17(2)	Ru(1)−C(2)−O(2)	175(2)
Ru(2)−C(3)	1.92(2)	C(3)−O(3)	1.11(2)	Ru(2)−C(3)−O(3)	175(2)
Ru(2)−C(4)	1.91(2)	C(4)−O(4)	1.13(2)	Ru(2)−C(4)−O(4)	176(2)
Ru(2)−C(5)	1.88(2)	C(5)−O(5)	1.15(2)	Ru(2)−C(5)−O(5)	175(2)
Rh(1)−C(6)	1.87(2)	C(6)−O(6)	1.13(2)	Rh(1)−C(6)−O(6)	178(2)
Rh(2)−C(7)	1.89(2)	C(7)−O(7)	1.12(2)	Rh(2)−C(7)−O(7)	178(2)
Ru(1)−C(B11)	2.06(2)	C(B11)−O(B11)	1.14(2)	Ru(1)−C(B11)−O(B11)	142.2(16)
Rh(1)−C(B11)	2.16(2)			Rh(1)−C(B11)−O(B11)	136.7(15)
Ru(1)−C(B12)	2.11(2)	C(B12)−O(B12)	1.16(2)	Ru(1)−C(B12)−O(B12)	142.8(14)
Rh(2)−C(B12)	2.15(2)			Rh(2)−C(B12)−O(B12)	137.3(14)
Ru(2)−C(B21)	2.18(2)	C(B21)−O(B21)	1.17(2)	Ru(2)−C(B21)−O(B21)	135.4(16)
Rh(1)−C(B21)	1.97(2)			Rh(1)−C(B21)−O(B21)	136.8(17)
Ru(2)−C(B22)	2.17(2)	C(B22)−O(B22)	1.22(2)	Ru(2)−C(B22)−O(B22)	134.4(13)
Rh(2)−C(B22)	1.93(2)			Rh(2)−C(B22)−O(B22)	136.7(14)
Rh(2)−C(B)	2.09(2)	C(B)−O(B)	1.14(2)	Rh(2)−C(B)−O(B)	137.7(16)
Rh(1)−C(B)	2.10(2)			Rh(1)−C(B)−O(B)	142.0(15)
Ru(2)−Ru(1)−C(1)	174.9(6)			Ru(2)−Ru(1)−C(2)	84.7(6)
Ru(1)−Ru(2)−C(3)	83.8(6)			Ru(1)−Ru(2)−C(4)	79.8(6)
Au−P(1)	2.287(5)	P(1)−C(111)	1.805(10)	P(1)−Au−Ru(2)	159.50(13)
		P(1)−C(121)	1.822(10)	P(1)−Au−Rh(1)	134.39(12)
		P(1)−C(131)	1.805(10)	P(1)−Au−Rh(2)	140.37(13)

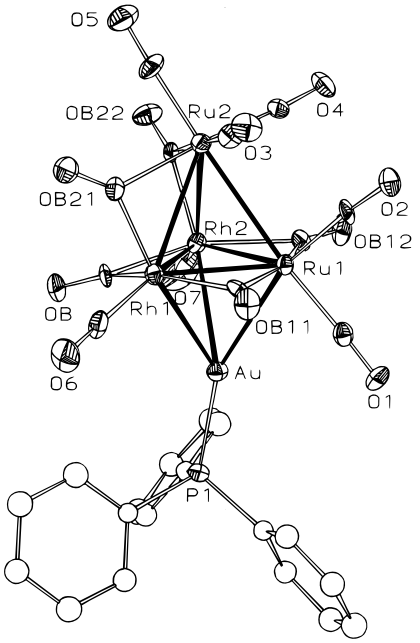

Figure 3. View of the $[Ru_2Rh_2(CO)_7(\mu_2\text{-}CO)_5(\mu_3\text{-}AuPPh_3)]^-$ anion (**3**). The C atoms of the carbonyl groups bear the same numbering as the respective connected O atoms. If the phenyl conformation is not taken into account, the anion has C_s idealized symmetry; the mirror plane contains the Ru(1), Ru(2), Au, P, C(1), O(1), C(2), O(2), C(B), and O(B) atoms.

label (Ru(1)) can be assigned to the metal at the short end of the asymmetric basal μ_2-CO bridges. Interestingly, the comparative analysis of the pattern of distances in the basal triangles of $[OsRh_3(CO)_7(\mu_2\text{-}CO)_5]^-$ (**4**) and **1** (Chart 1) verifies the relevance of charge equalization in mixed-metal clusters. As previously discussed,[13] the shortening of the Rh(1,2)−CB interactions in the basal plane of $[OsRh_3(CO)_7(\mu_2\text{-}CO)_5]^-$ compensates for the loss of valence electrons due to the bending

Chart 1. Comparison of the Bond Distances in the $M_3(\mu_2\text{-}CO)_3$ basal moiety of $[Ru_2Rh_2(CO)_7(\mu_2\text{-}CO)_5]^{2-}$ (**1**), $[Ru_2Rh_2(CO)_9(\mu_2\text{-}CO)_3(\mu_2\text{-}H)]^-$ (**2**), $[Ru_2Rh_2(CO)_7(\mu_2\text{-}CO)_5(\mu_3\text{-}AuPPh_3)]^-$ (**3**), and $[OsRh_3(CO)_7(\mu_2\text{-}CO)_5]^-$ (**4**)

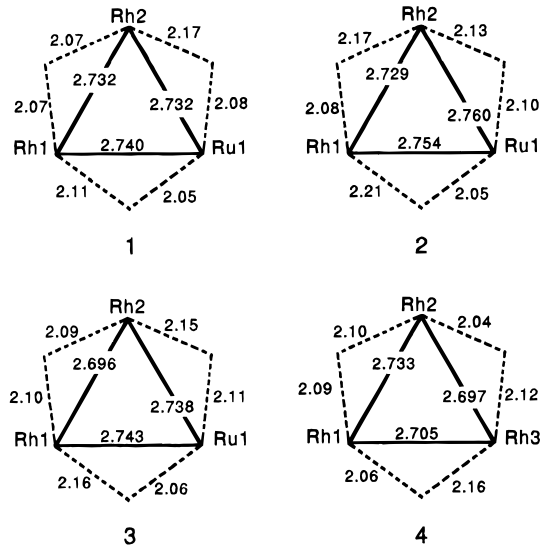

of two (formerly) equatorial terminal CO ligands toward the apical Os atom. This should hold also for **1**, which has a similar ligand stereochemistry; however, the presence of a formal Ru^- in the basal plane polarizes the $M_3(\mu_2\text{-}CO)_3$ moiety in the opposite direction in order to transfer some charge to the Rh atoms.[10] Obviously, the whole bridging carbonyl system will be affected by this process and the two basal−apical semibridging carbonyls become more asymmetric (Rh−C/Os−C 1.97/2.20 Å in **4** *vs* 1.91/2.30 in **1**), i.e. less bent toward the apical Ru atom. On the whole, the formal substitution of two Rh atoms with two Ru^- atoms promotes a deformation of the reference $[Rh_4(CO)_{12}]$ stereochemistry, resulting in a "loss of bonding" about the Rh atoms (and a consequent "increase of bonding" about the Ru ones). This clearly originates from the need for charge equalization. Moreover, if we look at the polyhedron defined by the oxygen atoms (Figure 4), it is evident that the packing efficiency of the CO ligands about the cluster core,

(13) Fumagalli, A.; Martinengo, S.; Ciani, G.; Moret, M.; Sironi, A. *Inorg. Chem.* **1992**, *31*, 2900.
(14) (a) Wei, C. H.; Wilkes, G. R.; Dahl, L. F. *J. Am. Chem. Soc.* **1967**, *89*, 4792. (b) Wei, C. H. *Inorg. Chem.* **1969**, *8*, 2384.

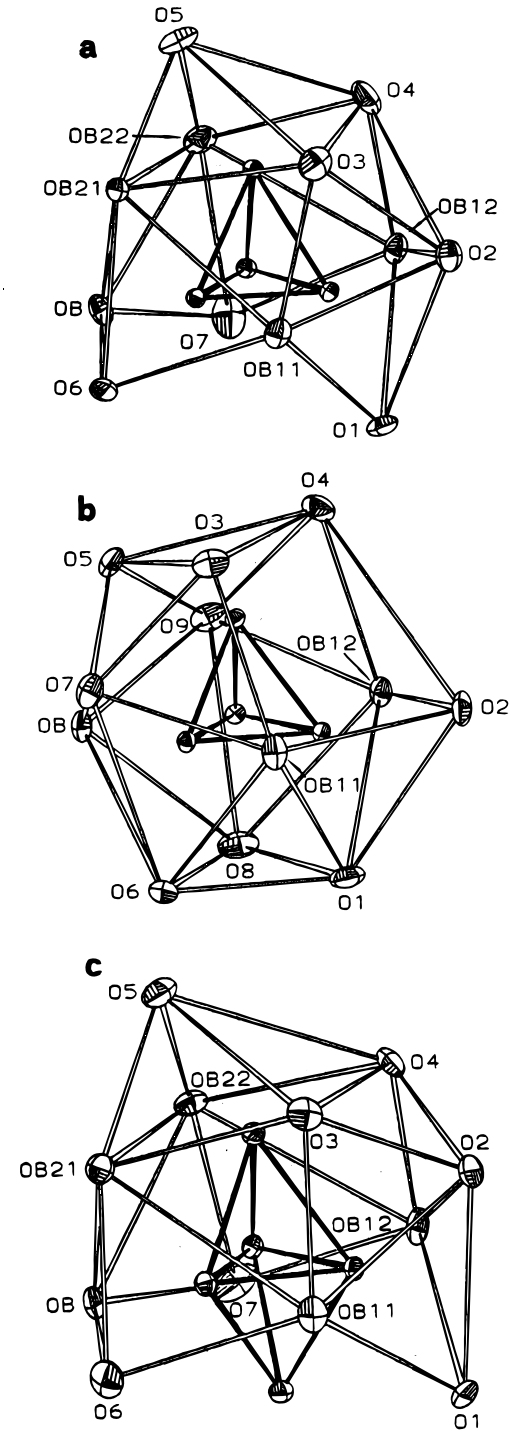

Figure 4. Ligand envelope obtained by joining the oxygen atoms closer than 5 Å; (a) $[Ru_2Rh_2(\mu_2\text{-}CO)_5(CO)_7]^{2-}$; (b) $[Ru_2Rh_2(\mu_2\text{-}H)(\mu_2\text{-}CO)_3(CO)_9]^-$; (c) $[Ru_2Rh_2(\mu_3\text{-}AuPPh_3)(\mu_2\text{-}CO)_5(CO)_7]^-$.

which play a central role in the ligand polyhedral model (LPM),[15] has little to do with the stereochemistry of **1** where the "loss of bonding" about the Rh atoms determines a large empty volume below the basal face.

Given the long Ru(1)−Ru(2) edge (which is, however, totally shielded by the carbonyl ligands) and the large hole in the ligand envelope, $[Ru_2Rh_2(CO)_7(\mu_2\text{-}CO)_5]^{2-}$ formally offers two possible "reactive" sites toward an incoming L^+. As a matter of fact, the reaction with H^+ affords **2**, where the H ligand is μ_2-bridging the Ru(1)−Ru(2) edge (Figure 2), while that with $AuPPh_3^+$ affords **3**, where the $AuPPh_3$ ligand is μ_3-bridging the basal Rh_2Ru moiety (Figure 3).

(15) Johnson, B. F. G.; Roberts, Y. V. *Polyhedron* **1993**, *12*, 977.

The similarity of the oxygen atom polyhedra of **1** and **3** (Figure 4a,c) confirms that the ligand hole below the basal face was substantially preformed and is large enough to accommodate the incoming $AuPPh_3$ after a moderate tilting of the two terminal COs bound to Ru(1), as shown by the decreasing of the Ru(2)−Ru(1)−C(2) bond angle from 101.1(4)° in **1** to 84.7(6) in **3**. In contrast, the μ_2-H bridging of the Ru(1)−Ru(2) edge largely perturbs the ligand envelope of the parent compound **1**. In fact, in order to create enough room about the Ru(1)−Ru(2) edge, the nearby carbonyl ligands must bend away, as shown by the widening of the Ru(1)−Ru(2)−C(3), Ru(1)−Ru(2)−C(4), and Ru(2)−Ru(1)−C(2) bond angles (from 76.4(5), 87.7(5), and 101.1(4)° in **1** to 108.4(3), 106.1(3), and 117.3(3)° in **2**, respectively). On the whole, this large perturbation drives the overall stereochemistry of **2** to resemble that of $[Rh_4(CO)_{12}]$ rather than that of the parent **1**. This is also apparent from the shape of the oxygen atom polyhedron of **2** (Figure 4b), which, in spite of a broken edge related to the presence of the hydridic ligand, has an almost icosahedral shape.

The intrabasal M−M bonds, which are all spanned by a bridging carbonyl (Chart 1), are similar in the three compounds, and as expected, the Ru−Ru bonds are slightly longer than the Rh−Rh ones. More interestingly, the behavior of the basal−apical M−M interactions and its dependence on the ligand stereochemistry deserve comment, since two common stereochemical rules seem to be violated. As a matter of fact, the Ru(2)−Rh bonds, which are spanned by a carbonyl in **1** and **3** but not in **2**, are on average longer in **1** and **3** (2.887 and 2.882 Å, respectively) than in **2** (2.731 Å); the Ru(2)−Ru(1) bond, which is spanned by a hydride in **2** but not in **1** and **3**, is shorter in **2** (2.898(1) Å) than in **1** and **3** (2.952(2) and 3.028(2) Å, respectively). On the other hand, if we compare the basal−apical M−M interactions within the same molecule, the pattern of bond lengths is coherent with the above-mentioned stereochemical rules, since the Ru(2)−Rh bonds are longer than the Ru(2)−Ru(1) bond in **1** and **3**, but the opposite holds for **2**. This suggests that the basal−apical M−M bond distances are under the control of both local and global ligand effects. Local effects concern the shortening or lengthening of a particular M−M bond spanned by a bridging carbonyl or hydride ligand, respectively. In contrast, global effects are those determined by the overall ligand stereochemistry. Clearly, in the case of **1** and **3**, the polarization of the ligand envelope toward the apical Ru atom (which supports five carbonyl ligands) determines a global ligand "repulsion" between the basal and the apical moieties which, judging from the observed bond distances, overcomes local effects.

This behavior confirms that the metal atom polyhedron may be regarded as the "soft core" of the molecule, capable of adapting itself to the demand of the surrounding ligands.

3. ^{1}H, ^{31}P and ^{13}C NMR Spectra. ^{13}C NMR spectra of the three species **1**−**3** were obtained in natural abundance or with samples enriched *ca.* 20% in ^{13}CO, as reported in the Experimental Section; most spectra were obtained from $[PPh_4]^+$ salts and occasionally from $[PPN]^+$ derivatives, with negligible difference in the chemical shifts.

(a) $[Ru_2Rh_2(CO)_{12}]^{2-}$. The $(PPN)^+$ salt under nitrogen in d_8-THF at 295 K shows in the carbonyl region one triplet at 222.6 ppm (J_{C-Rh} = 17.5 Hz); this is consistent with complete fluxionality of the 12 carbonyls over the entire cluster and coupling with both Rh atoms. Lowering the temperature does not yield a static structure, as was the case in the related $Rh_4(CO)_{12}$,[16] but only progressive broadening that at 167 K, very

(16) Cotton, F. A.; Kruczynsky, L.; Shapiro, B. L.; Johnson, L. F. *J. Am. Chem. Soc.* **1972**, *94*, 6191.

Table 4. Variable-Temperature ^{13}C NMR Spectra of $[Ru_2Rh_2(CO)_{12}AuPPh_3]^-$ as a $(PPh_4)^+$ or $(PPN)^+$ Salt in d_8-THF[a]

	203 K	253 K	293 K	323 K
C_1 (1 s)	206.8	206.7	206.4	
				206.3 (2 s)
C_2 (1 d)	206.4 {ca. 11}	206.3 {ca. 11}	206.0 {ca. 11}	
C_3, C_4 (2 s)	201.5	201.6	202.0	
C_5 (1 s)	197.4	197.6	198.1	198.6
C_6, C_7 (2 d)	202.7 [95.2]	202.6 [96.0]		
C_B (1 t)	255.0 [31.7]	253.7 [30]		
C_{B11}, C_{B12} (2 d)	259.6 [25.3]	258.3 [23.9]	256.4 [23.9]	254.6 [20]
C_{B21}, C_{B22} (2 d)	236.5 [42.3]	235.3 [46.1]		

[a] Integration and multiplicity are given in parentheses (s = singlet, d = doublet, t = triplet); δ in ppm, with $\{J_{C-P}\}$ and $[J_{C-Rh}]$ in Hz.

close to the freezing point of the solution, results in several broad undefined signals spread all over from 170 to 260 ppm.

A different behavior is observed if the sample is under 1 atm of CO, because of the reaction reported in eq 2; at *ca*. 170 K the characteristic doublet due to $[Rh(CO)_4]^-$ (205.2 ppm, J = 62.1 Hz) could be detected, together with a complex pattern which, although partially fluxional, gave evidence of bridging and terminal carbonyls. Raising the temperature to 295 K yielded the same triplet observed under nitrogen.

(b) $[Ru_2Rh_2(CO)_{12}H]^-$. ^1H NMR of $(PPh_4)[Ru_2Rh_2(CO)_{12}H]$ (**II**) in d_6-acetone gave at 303 K a hardly detectable high-field signal at δ *ca*. −20.0 ppm; in the temperature range 283−183 K a sharp singlet appeared in the correct 1:20 ratio with the $(PPh_4)^+$ signal, with a slight temperature shift from δ −19.6 to −20.0 ppm. The lack of ^{103}Rh coupling is consistent with the H atom bridging a Ru−Ru edge, as found in the crystal structure.

The ^{13}C NMR (^1H decoupled) spectrum of $(PPN)[Ru_2Rh_2(CO)_{12}H]$ in d_8-THF shows, at 173 K in the carbonyl region, a triplet at 208.0 ppm (J_{C-Rh} = *ca*. 17 Hz) and a singlet at 195.3 ppm, with an intensity ratio of *ca*. 3:1. In a spectrum where the ^1H coupling was maintained, the triplet appeared broad and ill-defined, while the singlet became a doublet (J_{C-H} = 10.6 Hz). The two resonances are observable up to room temperature (295 K).

The situation is consistent with two independent scrambling sets of, respectively, three and nine carbonyls. With reference to the structure of Figure 2, it may be observed that there is no CO bridging the upper $Ru(CO)_3$ moiety to the lower part of the molecule, whose nine carbonyls can therefore scramble independently on the Rh(1)−Rh(2)−Ru(1) triangle. The H atom, bridging in between, can interact with both systems, as confirmed by the decoupling experiment.

(c) $[Ru_2Rh_2(CO)_{12}(AuPPh_3)]^-$. ^{31}P NMR spectra of $(PPh_4)[Ru_2Rh_2(CO)_{12}(AuPPh_3)]$ (**III**) in d_6-acetone, in the temperature range 295−173 K, gave only two resonances which are correctly integrated as 1:1, a singlet at δ 24.0 ppm (PPh_4^+ cation), and a triplet ($^2J_{P-Rh}$ = 6.7 Hz) whose δ value varies with the temperature in the range 65.6−63.7 ppm; the last is consistent with the X-ray crystal structure, which locates the $AuPPh_3$ moiety on a Rh_2Ru face. The triplet appeared as a broad peak in ^{13}CO-enriched samples (*ca*. 20%) due to coupling with C_2 (see below).

^{13}C NMR spectra of **III** in d_8-THF, at low temperature (from 178 to *ca*. 250 K) are consistent with the idealized solid-state structure which, on the basis of C_s symmetry, yields eight groups of equivalent COs as reported in Table 4. As can be seen in the spectrum at 203 K reported in Figure 6 and in connection with the structure of Figure 3, the three low-field resonances may be easily assigned: the triplet at 255 ppm is due to the unique C_B bridging Rh(1) and Rh(2), and the two doublets have been assigned to the $C_{B11}-C_{B12}$ and $C_{B21}-C_{B22}$ Ru−Rh bridges, on the basis of the Rh coupling, which is expected to be larger for the shorter C−Rh interaction (see Table 3). In the terminal CO region the Rh-bonded C_6-C_7 may be easily associated with the typical doublet (J_{C-Rh} = 95 Hz) at 202.7 ppm; signal integration helps to assign the two sharp singlets at 197.4 and 201.6 ppm to C_5 and C_3-C_4, respectively, and the composite resonance at 206 ppm to C_1 and C_2. This resonance is derived by the superimposition of a singlet (C_1) and a doublet arising from the coupling of C_2 with phosphorus ($^3J_{C-P}$ = *ca*. 11 Hz) due to the almost linear sequence $C_2-Ru1-Au-P$.

At room temperature (293 K) the signals of C_6-C_7, C_B, and $C_{B21}-C_{B22}$ are lost in the background; this is consistent with the beginning of a fluxional process centered around the two Rh atoms. At 323 K, the highest temperature we could reach, the scrambling process does not reach completion but catches up also C_3-C_4. The resonances of C_1 and C_2 become unique with loss of the P coupling, while those of C_5 and $C_{B11}-C_{B12}$ are maintained, with some broadening. Noteworthy in this latter resonance is the temperature shift, which in the range 203−323 K is *ca*. 5 ppm.

Experimental Section

All operations were carried out under N_2 or CO as specified. Tetrahydrofuran was distilled from sodium−benzophenone and 2-propanol from aluminum isopropoxide. All other analytical grade solvents were degassed and stored under N_2. $(PPh_4)[Rh(CO)_4]$ and $(PPN)[Rh(CO)_4]$ were prepared by a modification of the published method,[17] using $K_3RhCl_6 \cdot 3H_2O$ instead of $RhCl_3 \cdot xH_2O$; $Ru_3(CO)_{12}$ was obtained commercially. Infrared spectra were recorded on a Perkin-Elmer 16 PC FT-IR spectrophotometer, using 0.1 mm CaF_2 cells previously purged with nitrogen. ^1H and ^{31}P NMR of anions **2** and **3** were obtained from pure samples of **II** and **III**. A sample of $(PPh_4)_2[Ru_2Rh_2(CO)_{12}]$ (**I**) for ^{13}C NMR was enriched (*ca*. ^{13}CO 20%) by exchange in THF solution with 90% ^{13}CO, using conventional vacuum line techniques; ^{13}CO-enriched anions **2** and **3** were synthesized, according to the reported methods, from enriched **I**. ^1H, ^{31}P, and ^{13}C NMR spectra were recorded respectively at 80.1, 81.0, and 50.3 MHz on Bruker instruments, with typical resolutions of ±2−3 Hz.

1. Synthesis of $(PPh_4)_2[Ru_2Rh_2(CO)_{12}]$ (I). $(PPh_4)[Rh(CO)_4]$ (770 mg, 1.39 mmol) and $Ru_3(CO)_{12}$ (295 mg, 0.46 mmol) were placed in a Schlenk tube under an N_2 atmosphere, and THF (40 mL) was added. After 24 h of stirring at room temperature, the red-brown solution was filtered to remove a small amount of brown precipitate, which prior to being discarded was washed twice with 1 mL of THF. The filtered solution with the collected washings was treated with 2-propanol (50 mL) and concentrated under vacuum (to *ca*. 70 mL) until there was formation of an abundant red microcrystalline precipitate; after stirring for 0.5 h more, the precipitate was allowed to settle. The mother liquor was removed with a syringe, and the precipitate was washed twice by decantation with 2-propanol (10 mL), discarding the washing. After vacuum drying, the product was redissolved in acetone (12 mL) and the solution was cautiously layered with 2-propanol (40 mL). When the diffusion was complete (*ca*. 1 week), after removal of the decanted mother liquor, the dark red crystals were washed thoroughly with 2-propanol, to remove a small amount of amorphous precipitate which

(17) Garlaschelli, L.; Della Pergola, R.; Martinengo, S. *Inorg. Synth.* **1991**, *28*, 211.

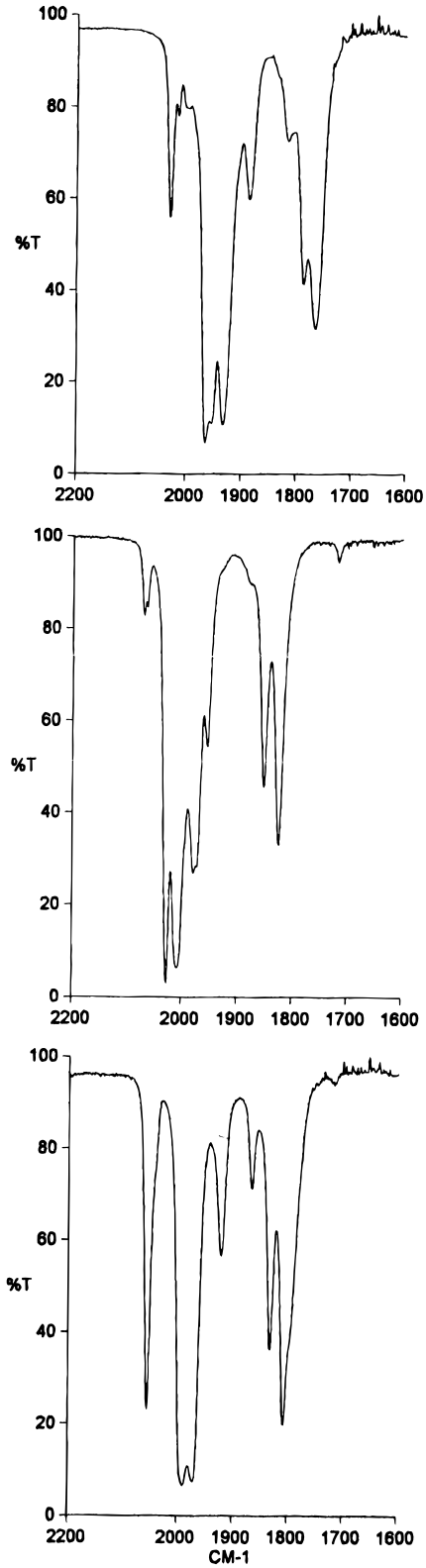

Figure 5. IR spectra in THF of $(PPh_4)_2[Ru_2Rh_2(CO)_{12}]$ (top), $(PPh_4)[Ru_2Rh_2(CO)_{12}H]$ (middle), and $(PPh_4)[Ru_2Rh_2(CO)_{12}AuPPh_3]$ (bottom).

remained suspended in the washings, and vacuum-dried; yield 574 mg (58%). Anal. Found: C, 51.05; H, 2.62. Calcd for $C_{60}H_{40}O_{12}P_2Rh_2Ru_2$: C, 50.65; H, 2.83. IR spectrum in THF (Figure 5): 2029 mw, 2015 w, 1963 s, 1952 s, 1931 ms, 1885 mw, 1815 w, 1786 m, 1764 ms (±2 cm^{-1}).

The crystals used for the X-ray structural determination were obtained by recrystallization from THF/2-propanol and contained clathrated THF.

A similar procedure, using $(PPN)[Rh(CO)_4]$, applies to the production

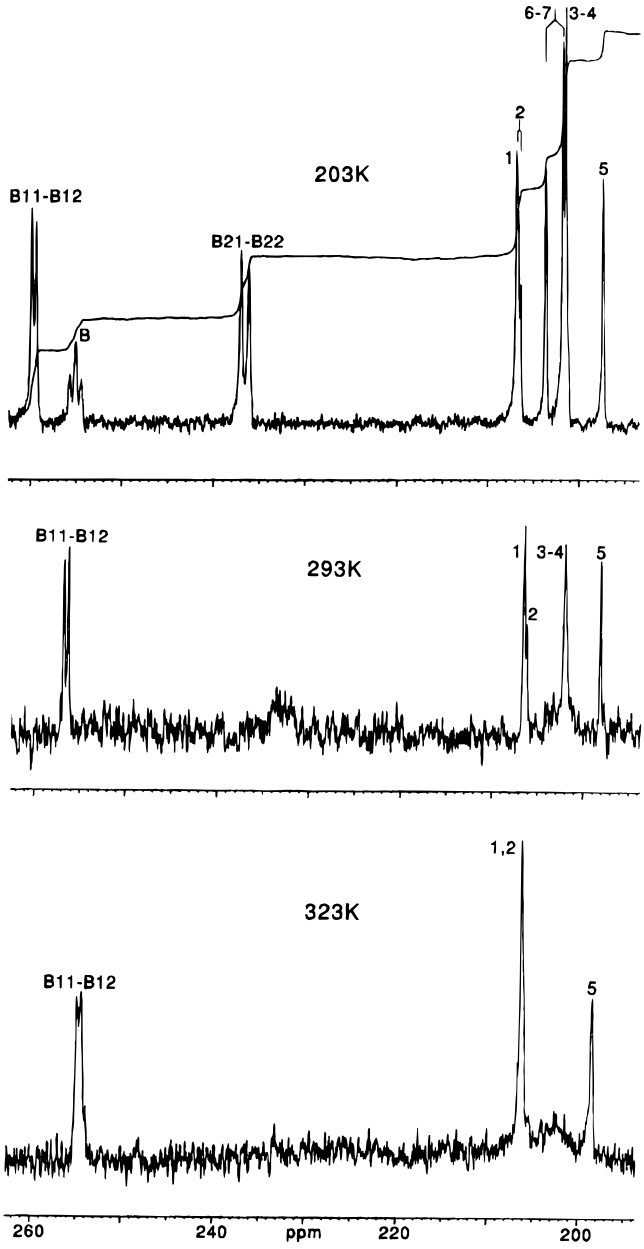

Figure 6. Variable-temperature ^{13}C NMR spectra of $(PPh_4)[Ru_2Rh_2(CO)_{12}AuPPh_3]$ in d_8-THF.

of the $(PPN)^+$ salt, which is obtained in comparable yield; the IR spectrum is almost identical with that of the $(PPh_4)^+$ derivative.

2. Synthesis of $(PPh_4)[Ru_2Rh_2(CO)_{12}H]$ (II). $(PPh_4)_2[Ru_2Rh_2(CO)_{12}]$ (274 mg, 0.19 mmol) was placed in a Schlenk tube under an N_2 atmosphere with THF (4 mL), and a slight excess of H_2SO_4 in THF solution (0.1 M, 1.2 mL) was added, with an immediate change of color from red to orange-yellow. The solution was filtered to remove a small amount of a white precipitate of $(PPh_4)_2(SO_4)$, which prior to being discarded was washed three times with 1 mL of THF. The volume of the solution was doubled by addition of *n*-hexane, which induced precipitation of a small amount of a tacky impurity; after 10 min of stirring, the decanted clear solution was transferred by syringe to another vessel and cautiously layered with some more *n*-hexane (50 mL). When the diffusion was complete (*ca.* 1 week), after removal of the decanted mother liquor, the dark yellow crystals were washed thoroughly with *n*-hexane and vacuum-dried; yield 71 mg (34%). Anal. Found: C, 37.23; H, 2.56. Calcd for $C_{36}H_{21}O_{12}PRh_2Ru_2$: C, 39.87; H, 1.95. IR spectrum in THF (Figure 5): 2070 w, 2064 w, 2027 s, 2007 s, 1979 ms, 1972 sh, 1954 mw, 1850 m, 1823 ms (±2 cm^{-1}).

3. Synthesis of $(PPh_4)[Ru_2Rh_2(CO)_{12}AuPPh_3]$ (III). $(PPh_4)_2[Ru_2Rh_2(CO)_{12}]$ (220 mg, 0.15 mmol) was placed in a Schlenk tube under an N_2 atmosphere with $AuPPh_3Cl$ (89.0 mg, 0.18 mmol); THF (5 mL)

Table 5. Summary of Crystal Data and Structure Refinement Parameters for $(PPh_4)_2[Ru_2Rh_2(CO)_{12}]\cdot C_4H_8O$ (I), $[PPh_4][Ru_2Rh_2(CO)_{12}H]$ (II), $[PPh_4][Ru_2Rh_2(CO)_{12}(AuPPh_3)]$ (III)

	I	II	III
formula	$C_{64}H_{48}O_{13}P_2Rh_2Ru_2$	$C_{36}H_{21}O_{12}PRh_2Ru_2$	$C_{54}H_{35}AuO_{12}P_2Rh_2Ru_2$
fw	1494.92	1084.46	1542.69
cryst syst	monoclinic	monoclinic	monoclinic
space group	$P2_1/n$	$P2_1/a$	$P2_1/n$
a, Å	11.256(2)	12.453(2)	11.720(2)
b, Å	26.712(2)	24.074(3)	13.133(3)
c, Å	20.048(5)	13.174(2)	35.614(2)
β, deg	90.45(2)	90.67(1)	95.70(1)
V, Å^3	6027(2)	3949(1)	5454(2)
Z	4	4	4
density (calc), g cm^{-3}	1.647	1.824	1.879
temp, K	293 (2)	293 (2)	293 (2)
abs coeff, mm^{-1}	1.146	1.670	3.932
goodness of fit on F_o^2 [a]	1.067	1.040	1.074
R1 and wR2 indices[b]	0.0483, 0.1085	0.0393, 0.0978	0.0539, 0.1268

[a] $[\sum w(F_o^2 - F_c^2)^2/(n - p)]^{1/2}$, where n is the number of reflections and p is the number of refined parameters. [b] $R1 = \sum||F_o| - |F_c||/\sum|F_o|$; $wR2 = [\sum w(F_o^2 - F_c^2)^2/\sum wF_o^4]^{1/2}$.

was added, and the mixture was stirred. After 1 h of reaction, the orange-yellow solution was filtered to remove a small amount of a white precipitate of $(PPh_4)Cl$, which prior to being discarded was washed twice with 1 mL of THF. The solution was treated, while it was stirred, with 2-propanol (7 mL) and *n*-hexane (2 mL) to induce precipitation of a small amount of a tacky impurity; after 10 min of stirring, the decanted clear solution was transferred by syringe to another vessel and cautiously layered with some more *n*-hexane (35 mL). When the diffusion was complete (*ca*. 1 week), after removal of the decanted mother liquor, the yellow crystals were washed thoroughly with *n*-hexane and vacuum-dried; yield 181 mg (78%). Anal. Found: C, 41.97; H, 2.02. Calcd for $C_{54}H_{35}AuO_{12}P_2Rh_2Ru_2$: C, 42.04; H, 2.29. IR spectrum in THF (Figure 5): 2055 ms, 1989 s, 1971 s, 1921 mw, 1865 w, 1831 m, 1807 ms (±2 cm^{-1}).

4. X-ray Analysis. (a) Collection and Reduction of X-ray Data. A suitable crystal of each compound was chosen and mounted on a glass fiber tip onto a goniometer head. Single-crystal X-ray diffraction data were collected on an Enraf-Nonius CAD4 diffractometer with the use of graphite-monochromatized Mo Kα radiation. The unit cell parameters and an orientation matrix relating the crystal axes to the diffractometer axes were determined by a least-squares fit of the setting angles of 25 randomly distributed intense reflections with $10° < \theta < 14°$. The data collections were performed by the ψ-scan method, at room temperature with variable scan speed and variable scan range. The crystal stability under diffraction conditions was checked by monitoring 3 standard reflections every 60 min. The measured intensities were corrected for Lorentz, polarization, background, and decay effects and reduced to F_o^2. An empirical absorption correction was applied using ψ-scans of three suitable reflections having χ values close to 90°.[18] For compound **III** a statistical absorption correction was also applied (DIFABS)[19]). Selected crystal data are summarized in Table 5.

(b) Solution and Structure Refinement. The structures were solved by direct methods (SIR92)[20] and difference Fourier methods. Compounds **I** and **II** were found to be disordered; for **I** a second metal tetrahedron slightly displaced from the other one was found, with occupancy factors 0.91:0.09, respectively, as obtained by refinement. Compound **II** shows instead a triangle of metal atoms staggered with respect to the Ru(2)Rh(1)/Rh(2) triangle (0.94:0.06 occupancy, respectively, as obtained by refinement), with Ru(1) completing the tetrahedron. No attempts to locate the COs of the minor components of the disordered metal frameworks were made. The structures were refined by full-matrix least squares against F_o^2 using reflections with $F_o^2 \geq 3\sigma(F_o^2)$ and the program SHELXL93[21] on a Silicon Graphics Indigo computer. Anisotropic displacement parameters were assigned to all atoms, excluding the minor components of the disordered metal frameworks in **I** and **II** (which were refined with a common isotropic displacement parameter), the phenyl carbon atoms, and the clathrated solvent molecule in **I**. All phenyl moieties were treated as rigid groups with hydrogen atoms riding on their parent carbon atoms and individual isotropic displacement parameters 1.2 times that of the pertinent carbon atom. In compound **2** the hydride ligand position was calculated by means of the program HYDEX[22] with $d_{M-H} = 1.80$ Å. The hydride was introduced in the final stages of F_o calculations but not refined.

Acknowledgment. We thank Mrs. M. Bonfà of the Università di Milano for recording the NMR spectra and the Ministero dell'Università e della Ricerca Scientifica e Tecnologica (MURST) for financial support.

Supporting Information Available: Tables giving full details of the X-ray data analyses, final atomic coordinates, anisotropic displacement parameters, and all bond lengths and angles (18 pages). Ordering information is given on any current masthead page.

IC950728U

(18) North, A. C. T.; Phillips, D. C.; Mathews, F. S. *Acta Crystallogr., Sect. A* **1968**, *24*, 351.
(19) Walker, N.; Stuart, D. *Acta Crystallogr., Sect. A* **1983**, *39*, 158.
(20) Altomare, A.; Cascarano, G.; Giacovazzo, C.; Guagliardi, A.; Burla, M. C.; Polidori, G.; Camalli, M. *J. Appl. Crystallogr.* **1994**, *27*, 435.
(21) Sheldrick, G. M. SHELXL-93, program for structure refinement; University of Göttingen, 1994.
(22) Orpen, A. G. *J. Chem. Soc., Dalton Trans.* **1980**, 2509.